Chalcogenide Letters Vol. 13, No. 11, November 2016, p. 489 - 505

ANOMALOUS ELASTIC AND OPTICAL BEHAVIOURS OF MIXED ELECTRONIC-IONIC OF xAg$_2$O−(35−x)[0.5MoO$_3$−0.5V$_2$O$_5$] −65TeO$_2$ CONDUCTOR GLASSES

M. ISMAIL[a], S. N. SUPARDAN[a], A. K. YAHYA[a], M. I. M. YUSOF[b*], M. K. HALIMAH[c]

[a]*School of Physics and Materials Studies, Universiti Teknologi MARA, 40450, Selangor, Malaysia*

[b]*Centre of Foundation Studies; Universiti Teknologi MARA Cawangan Selangor, Kampus Dengkil, 43800 Dengkil, Selangor, Malaysia*

[c]*Department of Physics, Faculty of Science, Universiti Putra Malaysia 43400, Selangor, Malaysia*

Ag$_2$O addition to quaternary xAg$_2$O-(35-x)[0.5MoO$_3$-0.5V$_2$O$_5$]-65TeO$_2$ (x = 0–25 mol%) glasses resulted in nonlinear behaviours with maxima at x = 10 mol% for ultrasonic velocities, independent elastic moduli and transition glass temperature (T_g). These results coincided with the electronic-to-ionic transition region as previously reported. A large decrease in elastic moduli beyond x = 10 mol% indicated a decrease in stiffness, thereby enabling ionic conductivity. Although Ag$_2$O addition weakened the glass network, the presence of MoO$_3$ played an important role as an additional glass former at $x \leq 10$ mol% apart from V$_2$O$_5$. Analysis of bulk compression and ring deformation models showed a large decrease in the ratio of theoretical to experimental bulk moduli (K_{bc}/K_e) at $x \leq 10$ mol% followed by near constancy with increased Ag$_2$O content. These results showed that ring deformation was reduced in the electronic region, but limited ring deformation took place in the ionic region, and that the main compression mechanism was mainly isotropic ring compression. Meanwhile, the optical energy gap (E_{opt}) and refractive index (n) showed a slope change at x = 10 mol% which confirmed the effect of mixed electronic–ionic conductivity on optical properties.

(Received August 30, 2016; Accepted November 2, 2016)

Keywords: Elastic moduli; Tellurite glass;Ultrasonic velocity; Optical energy gap; Glass transition temperature

1. Introduction

Among oxide glasses, tellurium oxide (TeO$_2$)-based glasses are receiving increased attention because of their optical and non-optical properties [1, 2], high refractive index [1, 3-5], good infrared transmission [6], high dielectric constant and electrical conductivity [7-9], good mechanical strength and chemical durability [10-12], and non-hygroscopic property compared to phosphate and borate glasses [13, 14]. These properties make TeO$_2$-based glasses suitable for various applications such as optical devices [15, 16], sensor system [17, 18], and CD memory devices [19]. TeO$_2$ glass consists of TeO$_4$ trigonal bipyramids (tbp) and TeO$_3$ trigonal pyramid (tp) unit structures with a lone electron pair in the equatorial position [1, 2, 11, 20, 21]. TeO$_2$ is known as a conditional glass former that requires the addition of modifier oxide, such as alkali, alkaline earth, and transition metal oxides, or another glass former to form an oxide glass with different structural units and oxide contents [10, 22]. The addition of modifiers or formers to the TeO$_2$ network causes the structural modification of Te, which transforms TeO$_4$ tbp to TeO$_3$ tp [2, 21-25].

In particular, the addition of several transition metal oxides with multivalent ions such as V$_2$O$_5$, CuO$_2$, MoO$_3$ and Fe$_2$O$_3$ on TeO$_2$ reportedly result in semiconductor properties and electronic conduction through polaron hopping from a lower cationic valence state to a higher one [25-29].

* Corresponding author: mohdi113@salam.uitm.edu.my

Meanwhile, studies on the addition of V_2O_5 (known to be a glass former) to tellurite glass in the form of binary vanadotellurite glass is gaining increased interest because of V_2O_5's glass-forming ability, conductivity, and semiconducting properties caused by the multivalency of V^{4+}/V^{5+}, which is an important criterion to be considered for electronic and industrial applications [26, 28, 30]. For a binary $x$$V_2O_5$–(100−$x$)$TeO_2$ glass system, the structural changes in the form of a continuous TeO_2 network take place at x < 20 mol%. Beyond 20 mol%, the TeO_2 network transforms into a vanadate network because of the formation of BO and causes an increase in the elastic moduli [13]. Moreover, in $x$$MoO_3$–(1−$x$)$TeO_2$ glass, MoO_3 has been reported to function both as a network modifier for x < 0.3 % with the formation of NBO and as a network former for x > 0.4 [31]. Studies on Ag_2O–MoO_3–TeO_2 glasses have reported that the enhancement in transition glass temperature (T_g) is attributed to the structural modification and the mixed glass former effect in the glass network [32]. A similar behaviour has also been observed in Li_2O–MoO_3–P_2O_5 [33], and Ag_2O–M_xO_y–TeO_2 (M_xO_y = WO_3, MoO_3, P_2O_5, and B_2O_3) glass systems [34]. The addition of MoO_3 as a third component in MoO_3–TeO_2–V_2O_5 glasses has been observed to increase the stability and rigidity of the glass network [26, 27, 35-38]. Moreover, optical studies on (60−x)V_2O_5–40TeO_2–$x$$MoO_3$ glasses have reported that the optical energy gap (E_{opt}) increased from 2.03 to 2.86 eV, and this increase is associated with a decrease in the NBO, which confirms the function of MoO_3 as a network former [27, 35].

Furthermore, the addition of a modifier oxide with monovalent ion, including alkali metal oxides such as Li_2O, Na_2O, and Ag_2O in tellurite glass, resulted in a more open structure of the glass network along with the formation of NBO, and the resulting material showed high ionic conductivity [39-42]. The addition of alkali metal oxides such as Li_2O, Na_2O, or Ag_2O coupled with a reduction of several multivalent transition metal oxides such as V_2O_5, MoO_3, CuO_2, or Fe_2O_3 in TeO_2 showed mixed electronic–ionic conductivity [43-50]. In particular, the addition of Ag_2O to vanadotellurite glass systems has become a subject of interest because of its high mobility and conductivity [34, 51-54]. Reports on Ag_2O addition to the ternary $x$$Ag_2O$–(1−$x$)$V_2O_5$–2$TeO_2$ glass system coupled with the reduction of V_2O_5 showed nonlinear conductivity behaviour involving transition from electronic to ionic state at x < 0.5 [46]. Moreover, non–linear conductivity behaviour with minimum conductivity was also reported for $x$$Ag_2O$–(50−$x$)$V_2O_5$–50$TeO_2$ [55, 56] and 10BaO–$x$$Ag_2O$–(85−$x$)$V_2O_5$–5$TeO_2$ [57] glass systems. Quite recently, studies on the conductive behaviour of $x$$Ag_2O$–(1−$x$)[0.5$V_2O_5$–0.5$MoO_3$]–2$TeO_2$ glasses with Ag_2O addition showed decreased electronic conductivity when x was increased to 0.4 followed by increased ionic conductivity at x > 0.4 [45]. This result is attributed to the electronic–ionic transition in the region and is linked with the structural transformation of VO_5 tbp to VO_4 tetrahedral and TeO_4 tbp to TeO_3 tp. Generally, structural changes are closely related to elastic properties and also to optical changes, which, when taken together, can provide additional insights about the function of Ag_2O in the glass system.

The ultrasonic velocity measurement technique, which is sensitive to glass network changes and compactness, is a useful tool in the study of elastic properties of glasses. Ultrasonic studies of several vanadotellurite glass systems such as $TeO_2V_2O_5$–Gd_2O_3 [6], MoO_3–TeO_2–V_2O_5 [36], (35−x)Na_2O–$x$$V_2O_5$–65$TeO_2$ [58], $x$$Li_2O$–35$V_2O_5$–(65−$x$)$TeO_2$ [59], (50−x)V_2O_5–$x$$Bi_2O_3$–50$TeO_2$ [30], 50(TeO_2)–(50−x)V_2O_5–x(TiO_2) [60], WO_3–(40−x)Ag_2O–60Te_2O [61] and (60−x)V_2O_5–xNiO–40TeO_2 [62] have been previously reported. These studies gave insight on how composition and type of oxide addition contribute to changes in rigidity and elastic moduli of the glass. In particular, an ultrasonic study on a ternary $x$$Ag_2O$–(50−$x$)$V_2O_5$–50$TeO_2$ glass system reported that the elastic stiffness decreases with increased Ag_2O content because of the formation of NBO [52]. Similarly, for quaternary $x$$Ag_2O$–(1−$x$) [0.5$V_2O_5$–0.5$MoO_3$]–2$TeO_2$ glasses, the electronic–ionic transition is also expected to affect the elastic properties [45]. Any structural changes around the electronic–ionic transition region are expected to be accompanied by changes in elastic properties [59]. Thus, elastic studies involving ultrasonic measurement can provide more detailed information not only on the stiffness and rigidity, but also on the cross-linking and ring deformation in the transition area around a mixed electronic–ionic conductivity environment. However, to our knowledge, reports on the elastic properties of $x$$Ag_2O$–(35−$x$)[0.5$MoO_3$–0.5$V_2O_5$]–65$TeO_2$ glass are unavailable.

Optical study can be a useful tool not only to investigate optically induced electronic transitions but to also provide information about the energy gap and band structure which can be linked to glass network modification [63-65]. A previous report on mixed alkali $(30-x)Li_2O–xK_2O–20Bi_2O_3–50B_2O_3$ [65] glass system, which is known to display mixed alkali effect (MAE) and is rather similar to the mixed electronic–ionic effect, reported a decrease in E_{opt} to a minimum value at x = 15 mol% before increasing with further addition of Li_2O. Meanwhile, the refractive index (n) showed a maximum value in the region. These results, which coincided with the expected MAE minima for the glass system, were suggested to provide evidence for the effect of MAE on optical properties. As such, given the close similarity between MAE and mixed electronic–ionic effects, the present $xAg_2O–(35-x)[0.5MoO_3–0.5V_2O_5]–65TeO_2$ glass system studied is expected to also display mixed electronic–ionic effect in optical properties. Furthermore, anomalous E_{opt} values have been reported for mixed electronic–ionic $50TeO_2–(50-x)V_2O_5–xK_2O$ glass system, and these anomalies hint at the possible presence of mixed electronic–ionic effect in optical properties [66]. However, reports on the optical properties for the $xAg_2O–(35-x)[0.5MoO_3–0.5V_2O_5]–65TeO_2$ mixed electronic–ionic glass system are unavailable.

In this work, the effect of Ag_2O on the structural, elastic, and optical properties of the $xAg_2O–(35-x)[0.5MoO_3–0.5V_2O_5]–65TeO_2$ glass system was investigated using FTIR spectroscopy, ultrasonic velocity and UV-vis spectroscopy, respectively. Additional analyses involving bulk compression and ring deformation models were performed to obtain more information about changes in the glass network under elastic compression.

2. Experimental

The quaternary $xAg_2O–(35-x)[0.5MoO_3–0.5V_2O_5]–65TeO_2$ glass was prepared using a standard melt-quenching method by mixing appropriate amounts of tellurium dioxide (TeO_2; 99.995% purity), vanadium pentoxide (V_2O_5; 99.95% purity), molybdenum oxide (MoO_3; 99.99% purity), and silver oxide (Ag_2O; 99.99% purity). The materials were weighed and mixed thoroughly by continuous grinding using an agate mortar and pestle to attain good homogeneity. The mixture was then placed in a porcelain crucible and heated at 1100 °C for 1 h in a box furnace. The melt sample was then poured in a stainless steel mould and annealed at 200 °C for 3 h. The annealed sample was then polished using fine sandpaper to produce a parallel opposite surface for ultrasonic velocity measurements.

X-ray diffraction (XRD) measurements were performed using an X' Pert Pro Panalytical diffractometer to confirm the amorphous nature of the samples. The density (ρ) of the glass samples was determined through Archimedes' method by using toluene as an immersion medium at room temperature. The molar volume (V_a) can be obtained using the equation below [52, 60]:

$$V_a = \frac{M_{glass}}{\rho_{glass}} \tag{1}$$

where M_{glass} is the molecular weight and ρ_{glass} is the density of the glass.

The infrared (IR) spectra of the glass samples were obtained using a Pelkin Elmer model spectrum One FTIR spectrometer in the wavenumber range of 400 cm^{-1} to 4000 cm^{-1} at room temperature. The FTIR data were fitted and deconvoluted using Gaussian peaks, and these deconvolution steps are typically repeated to attain the best results.

All ultrasonic velocity measurements in these studies were carried out using RAM-5000-M6 at 5 MHz in both shear and longitudinal modes by employing the linear least squares analysis of phase-versus-frequency at room temperature. The related elastic moduli were calculated using the equations below [52, 60]:

$$\text{Longitudinal modulus, } C_L = v_L^2 \rho \tag{2}$$

$$\text{Shear modulus, } \mu = v_S^2 \rho \tag{3}$$

$$\text{Bulk modulus, } K_e = C_L - \frac{4}{3}\mu \tag{4}$$

$$\text{Young's modulus, } E = \frac{9K_e\mu}{3K_e + \mu} \tag{5}$$

$$\text{Debye temperature, } \theta_D = \left(\frac{h}{k_b}\right)\left(\frac{3PN_A}{4\pi V_a}\right)^{\frac{1}{3}} v_m \tag{6}$$

$$\text{Poisson's ratio, } \sigma = \frac{C_L - 2\mu}{2(C_L - \mu)} \tag{7}$$

$$\text{Hardness, } H = \frac{(1-2\sigma)E}{6(1+\sigma)} \tag{8}$$

$$\text{Mean sound velocity, } v_m = \left[\frac{3v_L^3 v_S^3}{v_L^3 + v_S^3}\right] \tag{9}$$

where h is the Planck's constant, k_b is the Boltzmann's constant, N_A is Avogadro's number, V_a is the molar atomic volume, and P is the number of atoms in the chemical formula.

The optical absorption spectra of the glass powder samples were obtained using UV-visible spectroscopy Shimadzu UV-1650PC in the wavelength range of 200 nm to 800 nm at room temperature. The T_g values of all glass samples were obtained using a differential scanning calorimeter (NETZSCH, DSC 200 F3) at a heating rate of 10 °C min^{-1}.

3. Results

Fig. 1 presents the XRD patterns for all samples of $x$$Ag_2O$–(35−$x$)[0.5$V_2O_5$–0.5$MoO_3$]–65$TeO_2$ (x = 0–25 mol%) glass, and these patterns confirm their amorphous nature because no crystalline peaks are observed. The composition dependence of the experimental value of density (ρ) and the calculated molar volume (V_a) of the studied glasses are given in Table 1. From Fig. 2, ρ shows a moderate increase from 4492 kg m^{-3} (x = 0 mol%) to 4820 kg m^{-3} (x = 10 mol%) followed by a rapid increase from 5120 kg m^{-3} (x = 15 mol%) to 5970 kg m^{-3} (x = 25 mol%). By contrast, V_a shows a moderate decrease from 3.579 m^3 mol^{-1} (x = 0 mol%) to 3.478 m^3 mol^{-1} (x = 10 mol%) followed by a rapid decrease from 3.342 m^3 mol^{-1} (x = 15 mol%) to 2.981 m^3 mol^{-1} (x = 25 mol%) with gradual substitution of V_2O_5 and MoO_3 by Ag_2O.

The IR spectra of $x$$Ag_2O$–(35−$x$)[0.5$V_2O_5$–0.5$MoO_3$]–65$TeO_2$ (x = 0–25 mol%) glass system recorded at room temperature show six prominent bands in the regions 540–592, 621–697, 739–772, 829–882, 911–974, and 1060–1134 cm^{-1} (Fig. 3). Fig. 4 shows the deconvolution of the IR spectrum for x = 5 mol%. The peaks for the bands at 457–613 and 643–667 cm^{-1} are assigned to the symmetrical stretching vibration in the TeO_4 trigonal bipyramid (tbp) [67-69], whereas the peak at the 765–772 cm^{-1} band is assigned to the asymmetric stretching of the TeO_3 trigonal pyramid (tp) unit [64, 69, 70]. Meanwhile, the peaks at 882–883 [71, 72] and 829–841 cm^{-1} [27, 72, 73] are attributed to the stretching vibration of Mo–O–Mo tetrahedral units and MoO_4 tetrahedral units, respectively. Moreover, the peaks at 900–982 and 1055–1134 cm^{-1} are related to the stretching vibration of the VO_4 tetrahedral group and the stretching vibration of the V = O vanadyl group in the VO_5 tbp unit, respectively [69, 74]. When the amount of added Ag_2O was increased, the peaks at 1134 cm^{-1} shifted towards lower frequency, thereby indicating a decrease in BO number. In addition, the ratio of intensity and area of TeO_4 tbp to TeO_3 tp increases for $x \leq 10$ mol% but decreases for x > 10 mol%, thereby indicating the formation of BO and NBO, respectively.

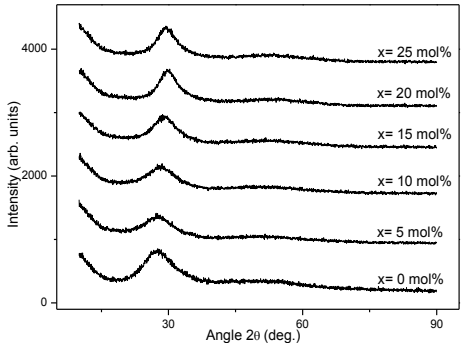

Fig. 1. XRD patterns of the $xAg_2O–(35−x)[0.5V_2O_5–0.5MoO_3]–65TeO_2$ (x = 0–25 mol%) glass samples

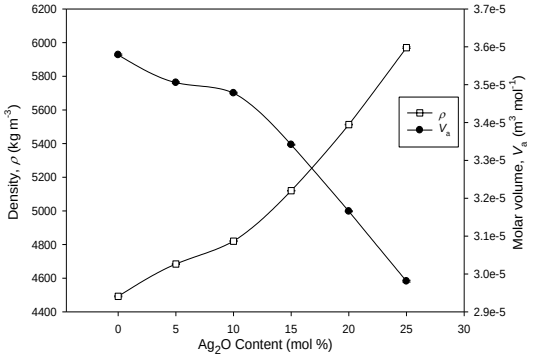

Fig. 2. Molar volume (V_a) and density (ρ) of the $xAg_2O–(35−x)[0.5V_2O_5–0.5MoO_3]–65TeO_2$ (x = 0–25 mol%) glass samples

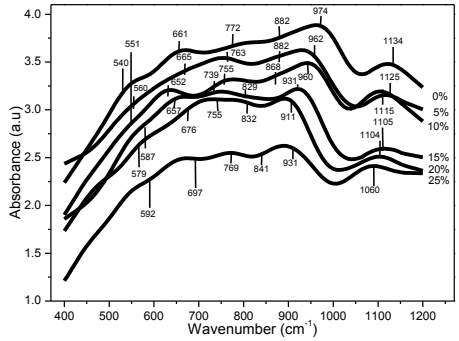

Fig. 3. IR spectra of the $xAg_2O–(35−x)[0.5V_2O_5–0.5MoO_3]–65TeO_2$ (x = 0–25 mol%) glass samples. Each spectrum has been shifted vertically for clarity

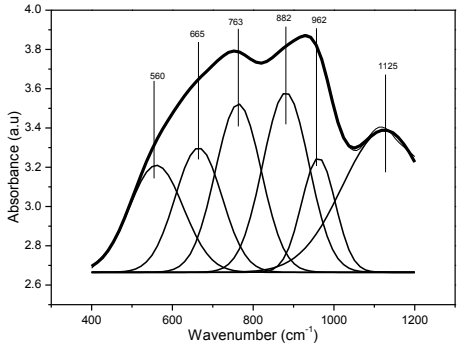

Fig. 4. Deconvulated FTIR spectra of $5Ag_2O–(30)[0.5V_2O_5–0.5MoO_3]–65TeO_2$

glass samples by using a Gaussian type function.

Table 1. Values of density (ρ), molar volume (V_a), longitudinal velocity (v_L), shear velocity (v_S), mean velocity (v_m), longitudinal modulus (C_L), shear modulus (μ), bulk modulus (K_e), Young's modulus (E), hardness (H), Debye temperature (θ_D), Poisson's ratio (σ) and transition glass temperature (T_g), of $xAg_2O–(35−x)[0.5V_2O_5–0.5MoO_3]–65TeO_2$ (x = 0–25 mol%) glass samples.

x (mol%)	0	5	10	15	20	25
ρ (kg m^{-3}) ± 2.83	4492	4684	4820	5120	5513	5970
V_a (m^3 mol^{-1}) × 10^{-5} ± 0.001	3.579	3.506	3.478	3.342	3.166	2.981
v_L (km s^{-1}) ± 0.01	3.27	3.41	3.49	3.32	3.16	3.03
v_S (km s^{-1}) ± 0.01	1.91	1.95	1.98	1.80	1.66	1.55
v_m (km s^{-1}) ± 0.01	2.60	2.66	2.70	2.47	2.29	2.14
C_L (GPa) ± 0.4	48.1	54.5	58.8	56.3	55.0	54.6
μ (GPa) ± 0.2	16.5	17.8	18.9	16.6	15.2	14.4
K_e (GPa) ± 0.6	26.2	30.9	33.5	34.3	34.7	35.5
E (GPa) ± 2.0	40.8	44.8	47.8	42.8	39.8	38.0
H (GPa) ± 0.3	2.9	2.9	3.0	2.3	1.9	1.7
θ_D (K) ± 0.4	311.3	317.0	319.8	292.6	272.9	257.6
σ ± 0.01	0.24	0.26	0.26	0.29	0.31	0.32
T_g (± 2 °C)	273	274	279	242	227	207

The measured values of longitudinal (v_L) and shear (v_S) velocities as well as the calculated values of the elastic moduli of the xAg$_2$O-(35-x)[0.5V$_2$O$_5$-0.5MoO$_3$]-65TeO$_2$ (x = 0–25 mol%) glass system are listed in Table 1. Ag$_2$O addition causes an initial increase in v_L and v_S from 3.27 km s^{-1} to 3.49 km s^{-1} and from 1.91 km s^{-1} to 1.98 km s^{-1} (for x = 0 mol% to 10 mol%), respectively, followed by a decrease in both v_L and v_S with further addition of Ag$_2$O (x > 10 mol%), as shown in Fig. 5. Meanwhile, from Fig. 6, both longitudinal (C_L) and shear (μ) moduli initially increase for x = 0 to 10 mol% then steadily decrease for x > 15 mol%. This variation trend is similar to that of the ultrasonic velocity. Detailed analysis revealed that C_L shows smaller decrease for x > 10 mol% compared to μ, which indicates that C_L is more dominant than μ. From Fig. 7, the Young's modulus (E) shows a similar behaviour to C_L and μ where it increases from 40.8 GPa (x = 0 mol%) to 47.8 GPa (10 mol%) and then decreases from 42.8 GPa (x = 15 mol%) to 38.0 GPa (for x = 20 mol%). By contrast, from Fig. 7, the bulk modulus (K_e) continues to increase from 26.2 GPa (x = 0 mol%) to 35.5 GPa (x = 25 mol%) with increased Ag$_2$O content.

From Table 1, the computed Poisson's ratio (σ) obtained from the elastic moduli shows a slight increase at $x \leq$ 10 mol% followed by a large increase for x > 10 mol%. Meanwhile, the hardness (H) is almost constant for x = 0 to 5 mol% before a small increase at x = 10 mol% and then a large decrease for x > 10 mol% with increased Ag$_2$O amount (Fig. 8). Fig. 9 shows that the Debye temperature (θ_D) and mean velocity (v_m) show similar trends with increased Ag$_2$O content. Thermal analysis results show that the transition glass temperature (T_g) increases from 273 °C (x = 0 mol%) to 279 °C (x = 10 mol%) and then decreases from 242 °C (x = 15 mol%) to 207 °C (x = 25 mol%) with increased Ag$_2$O content, as shown in Fig. 10.

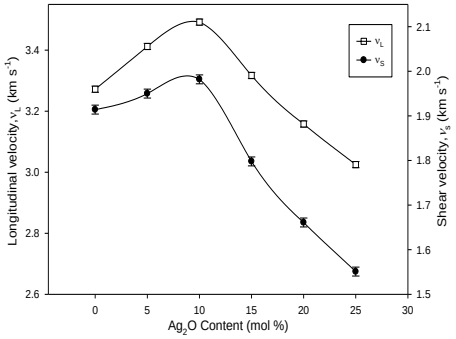

Fig. 5. Longitudinal and shear velocity versus Ag_2O content of the $xAg_2O–(35−x)[0.5V_2O_5–0.5MoO_3]–65TeO_2$ (x = 0–25 mol%) glass samples

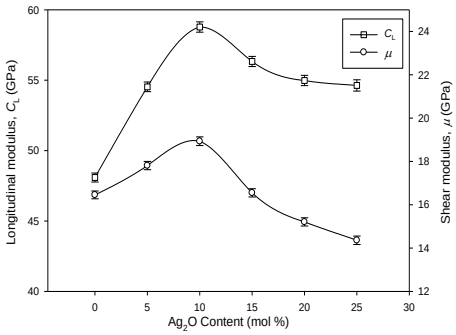

Fig. 6. Plot of longitudinal modulus (C_L) and shear modulus (μ) versus Ag_2O content of the $xAg_2O–(35−x)[0.5V_2O_5–0.5MoO_3]–65TeO_2$ (x = 0–25 mol%) glass samples

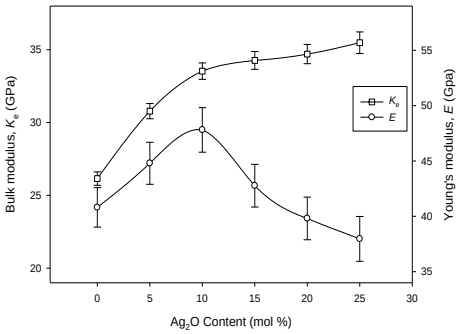

Fig. 7. Plot of bulk modulus (K_e) and Young's modulus (E) versus Ag_2O content of the $xAg_2O–(35−x)[0.5V_2O_5–0.5MoO_3]–65TeO_2$ (x = 0–25 mol%) glass samples

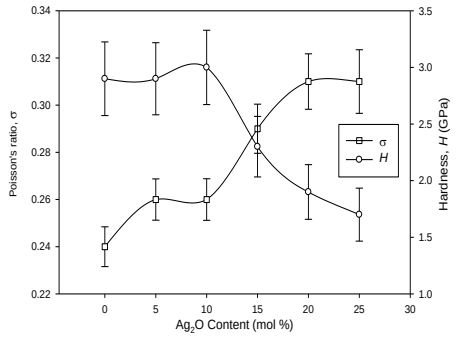

Fig. 8. Plot of Poisson's ratio (σ) and hardness (H) versus Ag_2O content of the $xAg_2O–(35−x)[0.5V_2O_5–0.5MoO_3]–65TeO_2$ (x = 0–25 mol%) glass samples

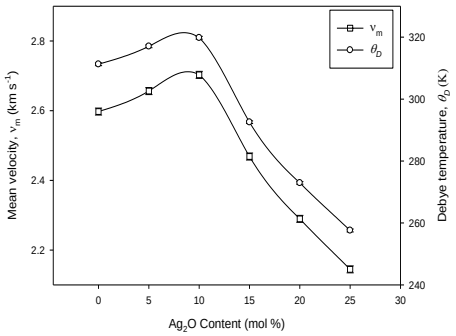

Fig. 9. Plot of Debye temperature (θ_D) and mean velocity (v_m) versus Ag_2O content of the $xAg_2O–(35−x)[0.5V_2O_5–0.5MoO_3]–65TeO_2$ (x = 0–25 mol%) glass samples

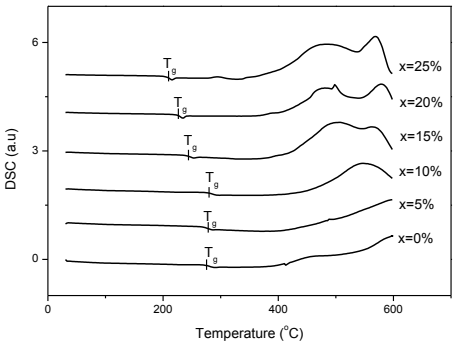

Fig. 10. DSC curves of the $xAg_2O–(35−x)[0.5V_2O_5–0.5MoO_3]–65TeO_2$ (x = 0–25 mol%) glass

Additional analyses involving bulk compression and ring deformation model were performed to obtain a clearer understanding of the experimental elastic behaviour and information about changes in the glass network of the $xAg_2O–(35−x)[0.5V_2O_5–0.5MoO_3]–65TeO_2$ system. According to this model, the ideal bulk modulus for an oxide glass can be expressed in the form [13, 75-80]:

$$K_{bc} = \frac{n_b r^2 F}{9} \tag{10}$$

where r is the bond length, F is the stretching force constant, and n_b is the number of network bonds per unit volume and is given by [13, 75-80]:

$$n_b = \frac{n_f N_A}{V_a} \tag{11}$$

where n_f is the number of network bonds per unit glass formula, N_A is Avogadro's number, and V_a is the molar volume. The stretching force constant, F, can be calculated by [13, 75-80]:

$$F = \frac{1.7}{r^3} \tag{12}$$

For polycomponent oxide glasses with i different types of network bonds, Equation 10 can be written as [13, 75-80]:

$$K_{bc} = \frac{N_A}{9V_a} \sum_i (x n_f F r^2)_i \tag{13}$$

where x is mole fraction of the oxide glass and F is the stretching force constant.

Table 2. Bond length r, stretching force constant (F), and coordination number (n_f) of Ag_2O, V_2O_5, MoO_3, and TeO_2

Oxide	r (nm)	F (N m^{-1})	n_f	References
Ag_2O	0.250	109	4	[21]
V_2O_5	0.183	277	5	[21]
MoO_3	0.196	226	6	[21]
TeO_2	0.199	216	4	[21]

The values of force constant, bond length, and coordination number of the oxide glass are listed in Table 2. The bulk compression model assumes that an isotropic deformation model leads to changes in the network bond length (l) and sizes without changing the bond angles. According to this model, bond compressions depend on the bond stretching force constant. Based on this model, when K_{bc}/K_e ratio is 1, the mechanism is pure isotropic ring compression. Meanwhile, for $K_{bc}/K_e > 1$, other compression mechanisms such as ring deformation may also be present [13, 75-80]. From Table 3, K_{bc} decreases to a minimum value at x = 10 mol% before increasing with increased Ag_2O content. Moreover, from Fig. 11, the ratio of K_{bc}/K_e sharply decreases from 2.82 (x = 0 mol%) to 2.14 (x = 10 mol%) before slightly increasing with increased Ag_2O content.

Table 3. E/G ratio, theoretical value of bulk modulus (K_{bc}), ratio of (K_{bc}/K_e), number of bond per unit volume (n_b), average ring size (ℓ), average stretching force constant ($\overline{F}$), and average crosslink density ($\overline{n}_c$) of xAg_2O–$(35-x)[0.5V_2O_5$–$0.5MoO_3]$–$65TeO_2$ (x = 0–25 mol%) glass samples.

x (mol%)	$\overline{F}$ (Nm^{-1})	K_{bc} (GPa) ± 0.04	E/G ± 0.1	K_{bc}/K_e ± 0.04	ℓ (nm) ± 0.008	$\overline{n}_c$
0	230	73.78	2.48	2.82	0.540	2.15
5	223	73.22	2.51	2.38	0.513	2.04
10	217	71.68	2.52	2.14	0.498	1.94
15	210	72.41	2.58	2.11	0.491	1.84
20	202	74.11	2.62	2.14	0.485	1.75
5	195	76.24	2.64	2.15	0.477	1.65

In the ring deformation model, the depression is not ideally isotropic because some parts of the ring may be deformed because of bending under compression.
The average ring size (ℓ) is given by [13, 75-80]:

$$\ell = \left[0.0106 \frac{\overline{F}}{K_e} \right]^{0.26} \tag{14}$$

where the average stretching force, $\overline{F}$ is given by [13, 75-80]:

$$\overline{F} = \frac{\sum (x n_f F)_i}{(x n_f)_i} \tag{15}$$

In our study, the calculated ℓ (Fig. 11) decreases with increased Ag_2O content, and a large decrease was observed from 0.491 nm (x = 0 mol%) to 0.477 nm (x = 10 mol%) followed by a slight decrease to 0.498 nm (x = 25 mol%) with increased Ag_2O content.

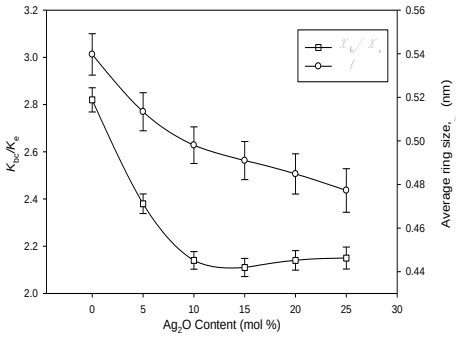

Fig. 11. Plot of K_{bc} / K_e ratio and average ring size (ℓ) with Ag_2O content.

The ideal crosslink density shows a decreasing trend from 2.15 to 1.65 with increased Ag_2O content, as listed in Table 3. The ideal crosslink density ($\overline{n}_c$) of the glass network is given by [13, 75-80]:

$$\overline{n}_c = \frac{1}{\eta}\sum_i (n_c)(N_c) \tag{16}$$

where n_c is the number of crosslink per cation, N_c is the number of cation per glass formula unit, and η is the total number of cations per glass formula unit.

The optical energy gap of the glass samples was calculated using the empirical relation given by [63, 81-83]:

$$\alpha(v) = B\left[\left(h\nu - E_{opt}\right)^2 / h\nu\right] \tag{17}$$

where α is the absorption coefficient, B is a constant, $h\nu$ is the incident photon energy, and E_{opt} is the optical energy band gap. The E_{opt} values were calculated by extrapolating the linear region of the plot of $(\alpha h\nu)^{1/2}$ against $h\nu$, where $(\alpha h\nu)^{1/2}$ = 0, as depicted in Fig. 12. The E_{opt} values that lie in the range of 1.014 eV to 1.404 eV (Table 4) increases with increased Ag_2O content. These E_{opt} values are also in reasonable agreement with the optical band gap values found in other tellurite glasses, such as $(60-x)V_2O_5$–$40TeO_2$–xSb_2O_3 [38], TeO_2–V_2O_5–NiO [84], and TeO_2-B_2O_3-ZnO [85].

Table 4. Optical parameters of xAg_2O–$(35-x)[0.5V_2O_5$–$0.5MoO_3]$–$65TeO_2$ (x = 0–25 mol%)

x (mol%)	E_{opt} (eV)	n
0	1.042	3.338
5	1.124	3.264
10	1.287	3.135
15	1.355	3.086
20	1.420	3.043
25	1.464	3.015

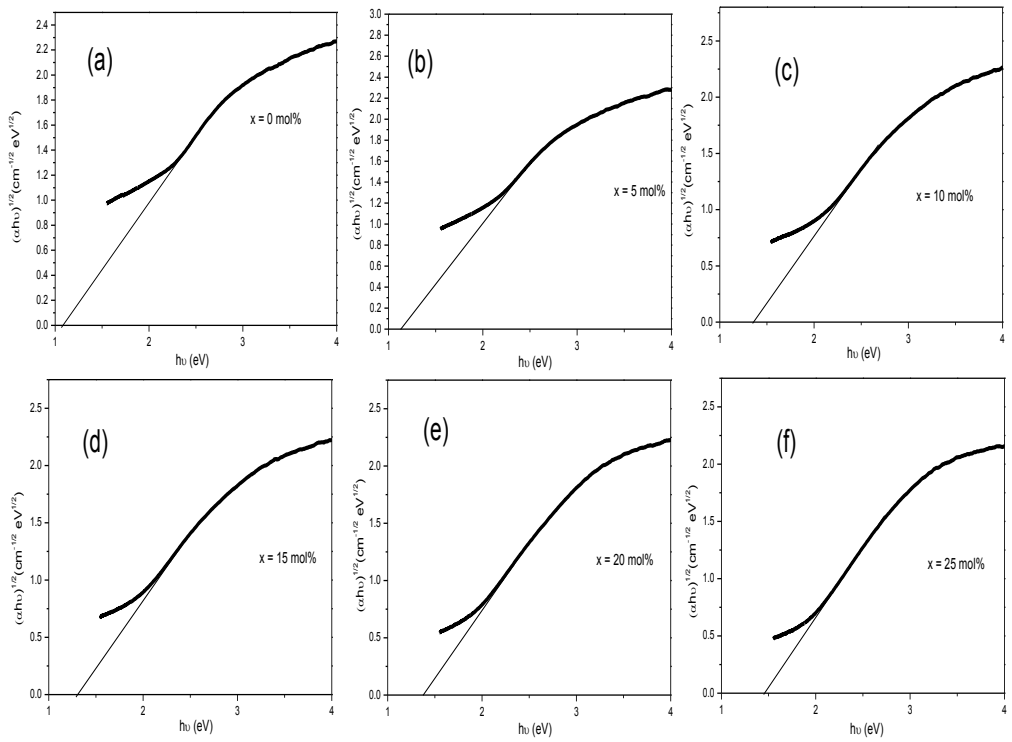

Fig. 12. $(\alpha h\nu)^{1/2}$ *as a function of energy (* $h\nu$ *) for* $xAg_2O–(35–x)[0.5V_2O_5–0.5MoO_3]–65TeO_2$ *(x = 0–25 mol%) glass*

Furthermore, the refractive index (n) was obtained from the optical energy gap using the following relation [63, 81-83]:

$$\frac{n^2-1}{n^2+2} = 1 - \sqrt{\frac{E_{\text{opt}}}{20}} \tag{19}$$

The variation in refractive index with Ag_2O content, as listed in Table 4, clearly shows a decrease in n with increased E_{opt} (Fig. 13).

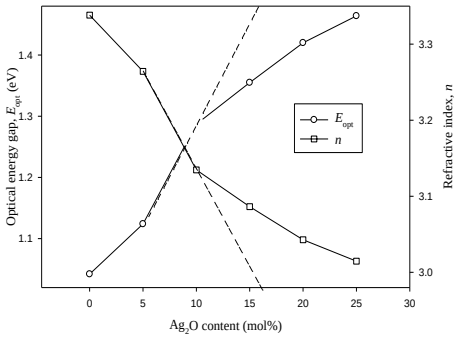

Fig. 13. Optical band gap (E_{opt} *) and refractive index (* n *) of* $xAg_2O–(35–x)[0.5V_2O_5–0.5MoO_3]–65TeO_2$ *(x = 0–25 mol%) glass. The dotted lines are just visual guides to show the slope change at x = 10 mol%.*

4. Discussion

The increase in density (ρ) in this study is probably related to the replacement of Ag_2O, which has a heavier molar mass (231.735 g mol^{-1}), with V_2O_5 and MoO_3, which have lower molar masses (181.88 g mol^{-1} and 143.94 g mol^{-1}, respectively). Moreover, changes in ρ may also be due to the decrease in the molar volume (V_a) of the glass (Fig. 2). A previous report suggested that other factors might affect the changes in V_a. Such factors include network modification, change in the ionic and atomic radii of ions, and difference in the molar volume of oxides [59, 60]. In the present work, the decrease in V_a may be due to the decrease in the number of VO_5 tbp and MoO_6 octahedra structural units involved in glass network formation alongside TeO_2 because V_2O_5 and MoO_3 was reduced in the glass formula. Ag_2O may not participate in the network formation because it is expected to function as a modifier. An increase in ρ accompanied by a decrease in V_a with Ag_2O replacing V_2O_5 has also been reported for Ag_2O-V_2O_5-TeO_2 [52] and quaternary Ag_2O-V_2O_5-MoO_3-TeO_2 glass systems . The density of the present $x$$Ag_2O$-(35-$x$)[0.5$V_2O_5-0.5MoO_3$]-65$TeO_2$ glass system was higher compared to that of $x$$Ag_2O$-(1-$x$)$V_2O_5$-$TeO_2$ glass [45], thereby suggesting that the presence of MoO_3 also results in a tight packaging of the original network.

Our FTIR result, which shows the presence of VO_4 tetrahedra, VO_5 tbp, MoO_4 tedrahedra, MoO_6 octahedra, TeO_3 tp and TeO_4 tbp, confirmed the formation of both BO and NBO in the glass network. For $x \leq 10$ mol%, the formation of BO indicated by the presence of TeO_4 tbp was more dominant compared to the effect of the reduction of MoO_6 octahedral and VO_5 tbp units. Although both MoO_3 and V_2O_5 were reduced in the chemical composition, TeO_2 is suggested to have a significant function as network former in the glass network for $x \leq 10$ mol% [86]. However, for x > 10 mol%, Ag_2O functions as a glass modifier, thereby weakening the glass network. In addition, MoO_3 also has an important function in structural modification because it functions as a network former for $x \leq 10$ mol% by forming MoO_6 octahedra and as a network modifier by forming MoO_4 tedrahedra for x > 10 mol% [72, 87].

The behaviours of v_L and v_S can be understood by the behaviours of independent moduli (C_L and μ) together with the variation in density according to the equations: $v_L = \sqrt{C_L / \rho}$ and $v_S = \sqrt{\mu / \rho}$ [58, 61]. Our results showed that the increase in both v_L and v_S for $x \leq 10$ mol% with increased ρ is strongly influenced by the changes in both C_L and μ, where the percentage of changes for both parameters are 22.3% and 14.3%, respectively. Moreover, the change in ρ was only 6.8% for the same glass composition. Meanwhile, for x > 10 mol%, both v_L and v_S rapidly decrease with increased ρ and a concurrent decrease in both C_L and μ. The reason for the observed initial increase in independent elastic modulus and other related moduli (Fig. 6-9) is primarily suggested to be related to the increase in BO, which strengthens the rigidity of the glass network. However, the decrease in elastic moduli for x >10 mol% indicates an increase in NBO, which decreases the rigidity of the glass. The gradual reduction of V_2O_5 and MoO_3 with increased Ag_2O content can be discussed by comparing findings of previous work on $x$$Ag_2O$-(50-$x$)$V_2O_5-50TeO_2$, where C_L, μ, and other elastic moduli were observed to decrease monotonically with increased NBO number [52]. Therefore, the increase in elastic moduli for $x \leq 10$ mol% in our present work indicates that MoO_3 in the $x$$Ag_2O$-(35-$x$)[0.5$V_2O_5-0.5MoO_3$]-65$TeO_2$ glass system functions as an additional network former, which results in a more compact glass and increased rigidity of the network. The significant effect of MoO_3 suggests that it is an intermediate, which is in agreement with findings in a previous report on ternary MoO_3-V_2O_5-TeO_2 glass [36].

The resistance of a material to uniform compression involving change in volume without change in shape was measured using bulk modulus (K_e). The observed sharp increase in K_e (Fig. 6) for $x \leq 10$ mol% with Ag_2O addition indicates a large decrease in compressibility. On one hand, a weak increase in K_e with further addition of Ag_2O for x > 10 mol% indicates a smaller decrease in compressibility; on the other hand, the sharp increase in Young's modulus (E) for $x \leq 10$ mol% indicates an increase in stiffness, and the subsequent drastic decrease for x > 10 mol% indicates a decrease in the stiffness of the network [61].

A previous study on conductivity of a vanado-tellurite glass system by R. A. Montani et. al reported that the existence of a deep minimum (x = 13.33 mol%) in the isotherm of conductivity of the $x$$Ag_2O$-(33.33-$x$)[0.5$MoO_3-0.5V_2O_5$]-66.67$TeO_2$ system corresponds to a change in the mechanism of the electrical transport process [45]. They reported that the decrease in electronic conductivity is due to the increase in vanadium-vanadium average distance between ions. Meanwhile, the increase in ionic conductivity for x > 13.33 mol% is due to the opening up of the glass network because of the increase in NBO, which makes ion displacement occur easily. This glass system, which has a composition similarly close to the glass system in the present study, showed a conductivity transition from the electronic to ionic state that is close to the elastic maximum observed in the present work. As such, in the present work, the observed changes in rigidity, which shows an increase for x < 10 mol% followed by a decrease for x >10 mol%, are presumed to be related to the mixed electronic–ionic effect. Therefore, besides structural changes, the elastic environment underwent drastic transformation leading to a more elastically relaxed environment for ionic conduction at higher Ag_2O contents. A similar case has been observed for 0.5[$x$$Ag_2O$-(1-$x$)$V_2O_5$]-0.5$TeO_2$ [55], (100-2x)TeO_2–$x$$Ag_2O$–$x$$WO_3$ [54], $x$$Ag_2O$-(1-x)[0.7$V_2O_5-0.3B_2O_3$] [88] and 10BaO–$x$$Ag_2O$–(85-$x$)$V_2O_5$–5$TeO_2$ [57] glass systems, in which a significant modification of the glass structure was closely linked to the transformation from mainly electronic to mainly ionic conduction with Ag_2O addition.

Poisson's ratio (σ) is defined as the ratio of lateral to longitudinal strain produced when tensile force is applied, and it is generally inversely proportional to the actual crosslink density in the glass network [13]. In glasses, the tensile strain produced in the network is unaffected by the crosslink density while the lateral strain significantly decreases with increased crosslink density [76]. In the present system, σ remains almost constant from x = 5 to 10 mol% of Ag_2O (Fig. 8), thereby indicating that the actual crosslink density did not change for $x \leq$ 10 mol%. Further addition of Ag_2O for x > 10 results in NBO formation, which causes σ to increase. This result indicates a low resistance towards lateral expansion. Meanwhile, hardness (H) indicates the resistance of a material to deformation and is influenced by changes in crosslink density, interatomic bond strength, and free volume. The large decrease in H for x > 10 mol% may be due to the modification of the glass network, which corresponds to the formation of NBO. As such, the decrease in H indicates the ease of eliminating free volume in the glass [24].

Furthermore, the Debye temperature (θ_D) is an important parameter that determines the extent of atomic vibrations in solid materials because it represents the temperature at which all modes of vibrations are excited and it also reflects the bond strength in a solid [6, 89]. From Equation (6), changes in θ_D depend on the changes in the number of atoms in the chemical composition (P), molar volume (V_a), and mean velocity (v_m). In this study, both P and V_a decrease and that both may not contribute to the nonlinear increase in θ_D. As such, in our work, the observed nonlinear increase in v_m, which shows a similar behaviour to θ_D (Fig. 9), indicates that the changes in θ_D are dominated by v_m, thereby reflecting the rigidity in the glass system. Moreover, the observed nonlinear behaviour of the glass transition temperature (T_g) (Fig. 10) confirms the changes in rigidity in the glass system [89]. The presence of MoO_3 in quaternary $x$$Ag_2O$-(1-$x$)[0.5$V_2O_5-0.5MoO_3$]-2$TeO_2$ also results in a larger T_g compared to ternary $x$$Ag_2O$-(1-$x$)$V_2O_5-2TeO_2$ [45], thereby indicating a larger internal energy barrier for chain mobility during glass transition was involved.

Additional analysis involving bulk compression together with the ring deformation model showed that a calculated bulk modulus K_{bc} value larger than K_e indicates that other mechanisms might be involved during compression, and these mechanisms require much less energy during compression . In general, K_{bc}/K_e is a measure of extent in which bond bending is governed by the configuration of the network bond, and this ratio is assumed to be directly proportional to the average ring size (ℓ) and inversely proportional to the experimental elastic moduli [79]. The value of ratio K_{bc}/K_e sharply decreases from 2.82 (x = 0 mol%) to 2.14 (x = 10 mol%) with the initial addition of Ag_2O, thereby indicating that ring deformation is reduced. Meanwhile, the ratio of K_{bc}/K_e is relatively constant around 2.1 with further addition of Ag_2O (x > 10 mol%), thereby

indicating that the main compression mechanism is still mainly isotropic ring compression because the K_{bc}/K_e values lie between 1 and 3. Moreover, the initial addition of Ag_2O ($x \leq 10$ mol%) resulted in a larger decrease in ℓ compared to that in ℓ for further addition of Ag_2O ($x > 10$ mol%) indicating decreased ring deformation . These variations in ℓ explains the behaviour of K_e .

Optical absorption edge study is an important tool to understand the optically induced transition and optical band gap of materials [63, 81-83]. In amorphous materials, indirect transition is more prominent compared to direct transition. The increase in NBO leads to a decrease in E_{opt} because the electron is bound less tightly and is easier to excite compared to the case in BO [63, 64, 84]. In present work, the sharp increase in E_{opt} for $x \leq 10$ mol% is suggested to be due to the increase in BO through the formation of TeO_4 tbp and VO_5 tbp. Meanwhile, for $x > 10$ mol% the slower increase in E_{opt} with further addition of Ag_2O was likely due to the slight reduction of BO with increased NBO fraction. Moreover, the structural modification that occurred with increased Ag_2O content results in a decrease in refractive index (n), and detailed analysis shows a slope change of n at $x = 10$ mol%, and this result reflects the changes in polarizability [5]. The opposite trends of E_{opt} and n were also observed for other tellurite glasses [63, 64, 84]. The changes in slope observed for E_{opt} and n at $x = 10$ mol% indicate that both quantities were also affected by electronic to ionic transition.

5. Conclusions

The effect of Ag_2O addition with concurrent reduction of both V_2O_5 and MoO_3 on the elastic, structural, and thermal properties of $x$$Ag_2O$-(35-$x$)[0.5$V_2O_5-0.5MoO_3$]-65$TeO_2$ glass was studied. Ag_2O addition at $x = 10$ mol% caused an initial increase in both longitudinal and shear velocities (v_L and v_S), both independent longitudinal and shear moduli (C_L and μ), Young modulus (E), Debye temperature θ_D, and transition glass temperature (T_g) before a sudden drop at $x > 10$ mol%. The observed nonlinear behaviours for elastic and thermal properties indicate rigidity changes, which coincide with the mixed electronic–ionic transition region, as previously reported. The increase in elastic moduli at $x \leq 10$ mol% were suggested to be due to the increase in BO, whereas the decrease in elastic moduli at $x \geq 15$ mol% was due to the increase in NBO. MoO_3 in this glass system behaves as a network former for $x \leq 10$ mol% and contributes to the enhancement of glass network rigidity before turning into a modifier for $x > 10$ mol%. Analysis involving bulk compression and ring deformation models showed a sharp decrease in K_{bc}/K_e ratio at $x = 10$ mol%, thereby indicating that ring deformation was reduced in the electronic region. Meanwhile, at $x > 15$ mol%, the K_{bc}/K_e values are nearly constant, thereby indicating that no further deformation took place in the ionic region. However, the main compression mechanism of the glass system was mainly isotropic ring compression. Meanwhile, optical energy gap (E_{opt}) and refractive index (n) showed slope changes at about $x = 10$ mol% with increased Ag_2O content. The slope changes indicated that the mixed electronic–ionic effect is also prevalent in the optical properties of the present glass system.

Acknowledgement

The authors are thankful to the Malaysia Ministry of Higher Education (MOHE) for funding this research under the Fundamental Research Grant Scheme (FRGS), 600-RMI/FRGS 5/3 (55/2014). The authors also thank the Faculty of Pharmacy, Universiti Teknologi Mara, Puncak Alam for providing an X-ray machine.

References

[1] J. Li, Z. Sun, X. Zhu, H. Zeng, Z. Xu, Z. Wang, J. Lin, W. Huang,R.S. Armstrong, P.A. Lay, Opt. Mater., **25**, 401 (2004).
[2] J. C. Sabadel, P. Armand, D. Cachau-Herreillat, P. Baldeck, O. Doclot, A. Ibanez, E. Philippot, J. Solid State Chem. **132**, 411 (1997).
[3] E. S. Yousef, J. Alloys Compd. **561**, 234 (2013).
[4] E.S. Yousef, B. Al-Qaisi, Solid State Sci. **19**, 6 (2013).
[5] S. Akamine, T. Nanba, Y. Miura, S. Sakida, in 9th Biennial Worldwide Congress on Refractories.
[6] Y. B. Saddeek, Mater. Chem. Phys. **91**, 146 (2005).
[7] M. M. Ahmad, E. S. Yousef, E. S. Moustafa, Physica B **371**, 74 (2006).
[8] T. Sankarappa, M. P. Kumar, G. B. Devidas, N. Nagaraja, R. Ramakrishnareddy, J. Mol. Struct., **889**, 308 (2008).
[9] M. Prashant Kumar, T. sankarappa, J. Non-Cryst. Solids **355**, 295 (2009).
[10] H. Desirena, A. Schülzgen, S. Sabet, G. Ramos-Ortiz, E. de la Rosa, N. Peyghambarian, Opt. Mater. **31**, 784 (2009).
[11] L. M. Sharaf El-Deen, M. S. Al Salhi , M. M. Elkholy, J. Alloys Compd. **465**, 333 (2008).
[12] J. Lin, W. Huang, Z. Sun, C. S. Ray, D. E. Day, J. Non-Cryst. Solids **336**, 189 (2004).
[13] M. A. Sidkey, R. El-Mallawany, R. I. Nakhla, A. A. El-Moneim, J. Non-Cryst. Solids **215**, 75 (1997).
[14] B. V. R. Chowdari, P. P. Kumari, J. Non-Cryst. Solids **197**, 31 (1996).
[15] V. K.Tikhomirov, A. B. Seddon, D. Furniss, M. Ferrari, J. Non-Cryst. Solids **326-327**, 296 (2003).
[16] S. Marjanovic, J. Toulouse, H. Jain, C. Sandmann, V. Dierolf, A. R. Kortan, N. Kopylov, R. G. Ahrens, J. Non-Cryst. Solids **322**, 311 (2003).
[17] N. Dewan, K. Sreenivas, V. Gupta, Sens. Actuators A **147**, 115 (2008).
[18] R. El-Mallawany, H. M. Diab, Physica B **407**, 3580 (2012).
[19] H. Hirashima, Michihisa IDE, T. Yoshida, J. Non-Cryst. Solids **86**, 327 (1986).
[20] M. S. Gaafar, M. A. M. Abdeen, S. Y. Marzouk, J. Alloys Compd. **509**, 3566 (2011).
[21] R. El-Mallawany Tellurite Glasses Physical Properties and Data, CRC Press, New York, 2002
[22] T. Hayakawa, M. Hayakawa, M. Nogami, P. Thomas, Opt. Mater. **32**, 448 (2010).
[23] W. Stambouli, H. Elhouichet, M. Ferid, J. Mol. Struct. **1028**, 39 (2012).
[24] M. Ismail, S. N. Supardan, A. K. Yahya, and R. Abd-Shukor, Int. J. Mater. Res. **106**, 1 (2015).
[25] A. Mekki, G. D. Khattak, L. E. Wenger, J. Non-Cryst. Solids **352**, 3326 (2006).
[26] D. Souri, M. Elahi, Phys. Scr. **75**, 219 (2007).
[27] D. Souri, Middle-East J. Sci. Res. **5**, 44 (2010).
[28] M. M. El-Desoky, M. S. Al-Assiri, Mater. Sci. Eng. **137**, 237 (2007).
[29] M. M. El-Desoky, J. Non-Cryst. Solids **351**, 3139 (2005).
[30] V. Rajendran, N. Palanivelu, B. K. Chaudhuri, K. Goswami, J. Non-Cryst. Solids **320**, 195 (2003).
[31] A. Mekki, G.D. Khattak, L. E. Wenger, J. Non-Cryst. Solids, **351**, 2493 (2005).
[32] B. V. R. Chowdari, P. P. Kumari, Journal Phys. Chem Solids, **58**, 515 (1997).
[33] L. Bih, M. El Omari, J. M. Reau, M. Haddad, D. Boudlich, A. Yacoubi, et al., Solid State Ionics **132**, (2000). 71.
[34] B. V. R. Chowdari, P. P. Kumari, Solid State Ionics **113-115**, 665 (1998).
[35] M. Elahi, D. Souri, Indian J. Pure & Appl Phy. **44**, 468 (2006).
[36] D. Souri, Measurement **44**, 1904 (2011).
[37] D. Souri, Measurement **44**, 717 (2011).
[38] D. Souri and K. Shomalian, J. Non-Cryst. Solids **355**, 1597 (2009).
[39] G. D. L. K. Jayasinghe, D. Coppo, P. W. S. K. Bandaranayake, J. L. Souquet, Solid State Ionics **76**, 297 (1995).
[40] D. Zhu, C. S. Ray, W. Zhou, D. E. Day, J. Non-Cryst. Solids, **319**, 247 (2003).
[41] M. L. F. Nascimento, S. Watanabe, Braz. J. Phys., **36**, 795 (2006).

[42] D. Dutta, A. Ghosh, Phys. Rev. B, **72**, 024201 (2005).
[43] M. Pant, D. K. Kanchan, P. Sharma, M. S. Jayswal, Mater. Sci. Eng. B, **149**, 18 (2008).
[44] R. A. Montani, M. A. Frechero, Solid State Ionics, **177**, 2911 (2006).
[45] R. A. Montani, M. A. Frechero, Solid State Ionics, **158**, 327 (2003).
[46] R. A. Montani, A. Lorente, M. A. Vincenzo, Solid State Ionics, **130**, 91 (2000).
[47] R. A. Montani, A. Lorente, M. A. Frechero, Solid State Ionics, **146**, 323 (2002).
[48] P. Rozier, T. Dubois, P. Salles, J. Non-Cryst. Solids, **311**, 241 (2002).
[49] G. D. L. K. Jayasinghe, M. A. K. L. Dissanayake, P. W. S. K. Bandaranayake, J. L. Souquet, D. Foscallo, Solid State Ionics **121**, 19 (1999).
[50] G. D. L. K. Jayasinghe, M. A. K. L. Dissanayake, M. A. Careem, J. L. Souquet, Solid State Ionics **93**, 291 (1997).
[51] E. C. Cardillo, R. A. Montani, M. A. Frechero, J. Non-Cryst. Solids **356**, 2760 (2010).
[52] R. El-Mallawany, A. Abousehly, E. Yousef, J. Mater. Sci. Lett. **19**, 409 (2000).
[53] B. V. R. Chowdari, P. P. Kumari, J. Mater. Sci. Lett., **33**, 3591 (1998).
[54] G. Upender, Ch. Ramesh, V. C. Mouli, Mater. Res. Bull., **46**, 199 (2011).
[55] H. M. M. Moawad, H. Jain, R. El-Mallawany, J. Phys. Chem. Solids **70**, 224 (2009).
[56] H. M. M. Moawad, H. Jain, R.El-Mallawany, T. Ramadan, M. El-Sharbiny, J. Am. Ceram. Soc. **85**, 2655 (2002).
[57] M. Pant, D. K. Kanchan, P. Sharma, Ionics **16**, 797 (2010).
[58] M. M. Umair, A. K. Yahya, Mater. Chem. Phys. **142**, 549 (2013).
[59] S. Laila, A. K. Suraya, A. K. Yahya, Chalcogenide Lett. **11**, 91 (2014).
[60] R. El-Mallawany, N. El-Khoshkhany, H. Afifi, Mater. Chem. Phys. **95**, 321 (2006).
[61] M. M. Umair, A. K. Yahya, M. K. Halimah, H. A. A. Sidek, J. Mater. Sci. Technol. **31**, 83 (2015).
[62] S. A. Salehizadeh, D. Souri, J. Phys. Chem. Solids **72**, 1381 (2011).
[63] G. Upender, S. Ramesh, M. Prasad, V. G. Sathe, V. C. Mouli, J. Alloys Compd. **504**, 468 (2010).
[64] E. A. Mohamed, F. Ahmad, K. A. Aly, J. Alloys Compd. **538**, 230 (2012).
[65] A. Agarwal, V. P. Seth, S. Sanghi, P. Gahlot, S. Khasa, Mater. Lett. **58**, 694 (2004).
[66] M. Farahmandjou, S. A. Salehizadeh, Glass Physics and Chemistry **39**, 473 (2013).
[67] S. K. J. Al-Ani, S. S. Al-Rawi, A. H. Jassim, H. A. Al-Hilli, Iraqi J. of Appl. Phys. **2**, 23 (2006).
[68] I. Z. Hager and R. El-Mallawany, J. Mater. Sci. **45**, 897 (2010).
[69] Y. B. Saddeek, I. S. Yahia, W. Dobrowolski, L. Kilanski, N. Romcevic, M. Arciszewska, Optoelectron. Adv. Mat. **3**, 559 (2009) .
[70] G. Upender, V. C. Mouli, J. Mol. Struct. **1006**, 159 (2011).
[71] Y. B. Saddeek, A. M. Abousehly, S. I. Hussien, J. Phys. D: Appl. Phys. **40**, 4674 (2007).
[72] R. Iordanova, L. Aleksandrov, A. Bachvarova-Nedelcheva, M. AtaaLa, Y. Dimitriev, J. Non-Cryst. Solids **357**, 2663 (2011).
[73] M. A. Frechero, O. V. Quinzani, R. S. Pettigrosso, M. Villar, R. A. Montani, J. Non-Cryst. Solids **353**, 2919 (2007).
[74] Y. Dimitriev, V. Dimitrov, M. Arnaudov, D. Topalov, J. Non-Cryst. Solids **57**, 147 (1983).
[75] B. Bridge, N. D. Patel, J. Mater. Sci. **21**, 1187 (1986).
[76] R. E. Mallawany, Mater. Chem. Phys. **53**, 93 (1998).
[77] A. Abd El-Moneim, Mohammed D. Alenezy, A. A. El-Namrouty, M. H. Badawi, E. G. El-Metwally, Phys. Chem. Glasses: Eur. J. Glass Sci. Technol. B **52**, 193 (2011).
[78] A. A. El-Moneim, Mater. Chem. Phys., **98**, 261 (2006).
[79] M. S. Gaafar, Y. B. Saddeek, L. A. El-Latif, J. Phys. Chem. Solids, **70**, 173 (2009).
[80] S. Y. Marzouk, Mater. Chem. Phys. **114**, 188 (2009).
[81] S. K. J. Al-Ani, C. A. Hogarth, R. El-Mallawany, J. Mater. Sci. **20**, 661 (1985).
[82] S. K. J. Al-Ani, A. A. Higazy, J. Mater. Sci. **26**, 3670 (1991).
[83] R. El-Mallawany, M. D. Abdalla, I. A. Ahmed, Mater. Chem. Phys. **109**, 291 (2008).
[84] D. Souri, S. A. Salehizadeh, J. Mater. Sci. **144**, (2009) 5800.
[85] J. N. Ayuni, M. K. Halimah, Z. A. Talib, H. A. A. Sidek, W. M. Daud, A. W. Zaidan, A. M. Khamirul, Mater. Sci. Eng. **17**, 012027 (2011).

[86] N. Baizura, A. K. Yahya, J. Non-Cryst. Solids **357**, 2810 (2011).
[87] L. S. Rao, M. S. Reddy, M. R. Reddy, N. Veeraiah, J. Alloys Compd. **464**, 472 (2008).
[88] M. Wasiucionek, B. Wnetrzewski, W. Jakubowski, Solid State Phenomena **39-40**, 297 (1994).
[89] Y. B. Saddeek and M. S. Gaafar, Mater. Chem. Phys. **115**, 280 (2009).